Article

Influence of Residual Amplitude and Phase Error for GF-3 Quad-Polarization SAR on Wind Vector Retrieval

Xiaochen Wang [1,2,3], Yuxin Hu [1,2,*], Bing Han [1,2], Xinzhe Yuan [4], Junxin Yang [1,2] and Jitong Duan [1,2]

1   Aerospace Information Research Institute, Chinese Academy of Sciences, Beijing 100190, China; wangxc@aircas.ac.cn (X.W.); hanbing@aircas.ac.cn (B.H.); yangjunxin18@mails.ucas.ac.cn (J.Y.); duanjt@aircas.ac.cn (J.D.)
2   Key Laboratory of Technology in Geo-Spatial Information Processing and Application Systems, Chinese Academy of Sciences, Beijing 100190, China
3   Laboratory of Target Microwave Properties (LAMP), Deqing Academy of Satellite Application, Huzhou 313200, China
4   The National Satellite Ocean Applications Center, Beijing 100081, China; arley_yuan@mail.nsoas.org.cn
*   Correspondence: huyx@aircas.ac.cn

Abstract: High-resolution wind vector is important to investigate local winds' variability over the global ocean. Quad-polarization Synthetic Aperture Radar (SAR) can provide wind vector independently without any external wind direction inputs. Although quad-polarization SAR wind retrieval algorithms have been widely studied, improvements are still required. The amplitude and phase imbalance of polarization channel cannot be neglected for improving the wind vector retrieval precision. In this study, rainforest was performed to remove the amplitude and phase imbalance of polarization channel of GF-3 SAR. To explore the applicability of this method for sea surface measurement, the influence of residual amplitude and phase error for GF-3 quad-polarization SAR on wind vector retrieval was assessed. Variation of amplitude and phase imbalance of sea surface for transmit and receive channel were assessed against collocated wind speed and incidence angle. Considering the polarization difference of VV channel relative to HH channel, the residual amplitude and phase error was found to be closely related to wind speed and polarization isolation. Correction of residual amplitude and phase error were employed to improve the retrieval precision of wind vector. It is revealed that the wind speed retrieval precision of VV polarization improved with correction of residual amplitude error. In addition, the influence of residual amplitude and phase error on wind direction retrieval can be neglected. Thus, it is concluded that correction of amplitude and phase error has the potential to improve wind vector retrievals from GF-3 quad-polarization SAR.

Keywords: GF-3 quad-polarization SAR; wind vector; residual amplitude and phase error

1. Introduction

Observation of wind vectors is important to explore the mechanism of ocean surface dynamics circumstance and air-sea interaction effect. Of which, Synthetic Aperture Radar (SAR) performs great capabilities of wind vector retrieval, as remote sensing radars, due to its characteristic of high-resolution, not affected by clouds, can work all day and night [1–3]. To acquire precise wind field information, an empirical relationship between radar backscatter and wind vector was iteratively optimized by a large accumulation of Normalized Radar Cross Section (NRCS) and collocated wind vectors at 10 m above sea surface U_10. The semi-empirical geophysical model functions (GMF), namely CMOD, works well for C band spaceborne scatterometer and SAR [4,5]. However, SAR operates in a fixed azimuth direction, which results that wind speed and direction cannot be acquired simultaneously from single SAR imagery [6,7]. To inverse wind speed from SAR imagery, the matched wind direction needs to be provided for removal of azimuth ambiguity. Recent study revealed the capability of quad-polarization SAR for wind speed and wind direction

retrieval. It is validated that the C-2PO model was used to acquire wind speed, and wind speed was substituted into CMOD5.N to obtain uncertainty wind direction, and polarization correlation coefficient was used to eliminate the ambiguity of wind direction [8]. However, few studies focused on this issue due to the lack of enough quad-polarization SAR data and the unsatisfying precision of wind direction retrieval, which has instead deteriorated the retrieval precision of wind speed [9–11].

Since August 2016, GaoFen-3 (GF-3) was launched and operated to acquire scenes of ocean surface with 12 types of observation modes. Comparing with other orbited C band SAR sensors, such as RADARSAT-2, Sentinel, etc., the GF-3 wave mode works with quad-polarization mode, which provides great convenience for wind vectors' retrieval. In previous study, empirical methods for wind speed retrieval were explored using GF-3 SAR imagery [12–14]. It is validated that the acquisition of GF-3 SAR can be well applied for wind speed retrieval. Although it is claimed that the GF-3 SAR has been well calibrated by field active calibrator, the existence of GF-3 SAR error sources still affect the quantitative application of wind field retrieval. For GF-3 polarization SAR system, the error sources which affect the precise scattering measurement of radar echo can be concluded as five parts: (1) amplitude and phase imbalance introduced by transmit channel and receive channel respectively; (2) sampling time delay difference caused by transmission channel and reception channel delay; (3) crosstalk and amplitude phase imbalance of antenna; (4) polarization deflection angle introduced by satellite attitude; (5) faraday rotation angle introduced by ionosphere. Recent study revealed that the error sources of GF-3 polarization SAR were important and the influence of each part on signal propagation was given [15,16]. Some studies proposed the effect of GF-3 SAR system errors on polarization decomposition and further imagery classification [17–19]. It is found that the influence of amplitude and phase error can be neglected when in terms of GF-3 quad-polarization SAR classification and mapping. However, few studies have focused on its influence on quantitative remote sensing inversion. Among all five mainly error sources, the amplitude and phase imbalance were dominated in total polarization SAR errors. In consideration of target backscattering characteristics, it is important to assess the influence of residual amplitude and phase error from amplitude and phase imbalance for further remote sensing application, especially for wind vector retrieval. Therefore, the calibration and the correction of the residual amplitude and phase error is very important to acquire precise NRCS from ocean surface.

Generally, collocation of active radar calibrator and corner reflector was recognized as an effective way of SAR calibration [20]. Until now, it is also revealed that the methods using natural scene (rainforest etc.) works well to calibrate the precise NRCS of single polarization SAR, especially for qualitatively ocean remote sensing [13,21]. Meanwhile, the quad-polarization channel error also can be removed using polarization distortion matrix extracted from SAR imagery of rainforest. However, the bias caused by residual amplitude and phase error of quad-polarization SAR channel is still in doubt, especially for qualitatively ocean remote sensing application. Few studies focused on the qualitative assessment of residual amplitude and phase error on wind vector retrieval. To perform high-precision wind vector retrieval, it is worthwhile to investigate the influence of residual amplitude and phase error on ocean surface wind vector retrieval.

In this paper, the qualitative assessment of influence of residual amplitude and phase error on wind vector retrieval was proposed. The method of amplitude and phase correction using matched rainforest dataset is presented in Section 2. A brief illustration of potential of sea surface for SAR amplitude and phase correction was also presented. In Section 3, the SAR amplitude and phase imbalance of sea surface relative to wind speed and incidence angle was proposed. Considering sea surface scattering in a different polarization channel, the residual amplitude and phase error was present. In addition, the influence of residual amplitude error on wind vector retrieval was proposed and validated. In Section 4, the influence of residual phase on wind direction retrieval was discussed.4. The conclusions are given in Section 5.

2. Materials and Methods

2.1. Materials

The GF-3 SAR wave mode imagery from August 2018 to November 2019 were acquired and collocated with European Centre for Medium-range Weather Forecasting (ECMWF) data. ECMWF provides meteorology and oceanography data assimilation results, with a spatial resolution of 0.125° and temporal resolution of 6 h. The wind speed above 10 m height from sea surface U_10 was provided as on-site measurement. Considering the mismatch of spatial and temporal resolution for used datasets, interpolation was performed for acquisition in the same scale. Pixel spacing of 1 km was performed to collect GF-3 SAR imagery for retrieval precision. Time interval between SAR imaging and on-site measurement less than 30 min was taken as a valid dataset. The parameters of used GF-3 SAR wave mode imagery were listed in Table 1. It is noticed that the coverage of GF-3 SAR wave mode imagery can provide 5 km × 5 km swath width for every 50 km along the orbit direction. The collected GF-3 data were matched with ECMWF data. The map of collected GF-3 SAR wave mode imagery location is shown in Figure 1.

Table 1. Parameters of used datasets in this study.

Parameters	Values
Frequency	5.4 Ghz
Incidence angle	36.1°/22.1°/39.6°
Polarization	HH/HV/VH/VV
Resolution	10 m
Swath	5 km
Number of data	2300
Acquision time	2018,9–2019,9
U_{10}	0–20 m/s, provided by ECMWF
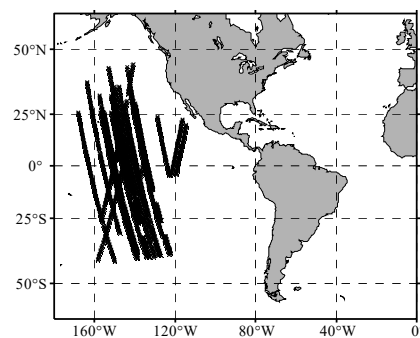
Figure 1. Map of collected GF-3 SAR wave mode imagery.

2.2. Methods

Theoretically, the H-polarization and V-polarization electromagnetic waves are transmitted through two different channels, which perform the same effects on amplitude and phase of radar echo. However, due to the achievement of hardware equipment, the effect of channel on H-polarization and V-polarization radar echo was not the same, and so are the receive channels of H-polarization and V-polarization electromagnetic waves. This makes the amplitude and phase imbalance between the transmit channel and receive channel of V-polarization electromagnetic waves relative to the transmit and receive channel of H-polarization electromagnetic wave, resulting in distortion of polarization measurement. To remove the effect of crosstalk and amplitude phase imbalance on quad-polarization

SAR imagery, the quad-polarization calibration method was usually performed, which was followed as:

$$\begin{bmatrix} M_{HH} & M_{HV} \\ M_{VH} & M_{VV} \end{bmatrix} = Ae^{j\theta}R^TST = Ae^{j\theta}\begin{bmatrix} 1 & \delta_1 \\ \delta_2 & f_r \end{bmatrix}\begin{bmatrix} S_{HH} & S_{HV} \\ S_{VH} & S_{VV} \end{bmatrix}\begin{bmatrix} 1 & \delta_3 \\ \delta_4 & f_t \end{bmatrix} \tag{1}$$

where, A and θ are the absolute amplitude and phase factors of the system, M represents the ground object polarization scattering matrix measured by multi-polarization radar, M_{ij} represents the echo transmitted by j polarization and received by i polarization, R is the receive distortion matrix and T is the transmit distortion matrix, S represents the real scattering matrix of ground object target.

To calibrate the quad-polarization SAR, the scattering matrix of the ground object is acquired on the basics of some artificial point targets in our field calibration process. Regular geometry with simple known scattering mechanisms can be used to acquire the polarization distortion. Generally, the polarization active radar calibrators (PARC) method is widely used to solve the matrix of crosstalk and amplitude-phase imbalance [22]. However, the performance of natural ground and artificial point targets were significantly different in SAR scattering, which caused scattering errors in SAR calibration. It was proven that natural ground targets behaved much better for quantitative remote sensing application.

(1) Rainforest

Recent study revealed that the natural distributed ground targets can be performed to calibrate the GF-3 quad-polarization SAR. Assuming that the scattering of rainforest follows the reciprocity and reflection symmetry theory, the phase error between different polarization channels and crosstalk were calibrated using four polarization SAR imagery of rainforest.

$$\begin{aligned} phase\left(S_{HV}^*S_{VH}\right) &= 0 \\ phase(S_{HH}^*S_{VV}) &= 0 \end{aligned} \tag{2}$$

Then the relative amplitude and phase between different polarization channels can be calibrated. Following the reciprocity of system, the $\delta_1 = \delta_4$, $\delta_2 = \delta_3$, $f_r = f_t = f$, then the Equation (1) can be simplified as:

$$\begin{bmatrix} M_{HH} & M_{HV} \\ M_{VH} & M_{VV} \end{bmatrix} = Ae^{j\theta}\begin{bmatrix} 1 & \delta_1/f \\ \delta_2 & 1 \end{bmatrix}\begin{bmatrix} 1 & 0 \\ 0 & f \end{bmatrix}\begin{bmatrix} S_{HH} & S_{HV} \\ S_{VH} & S_{VV} \end{bmatrix}\begin{bmatrix} 1 & 0 \\ 0 & f \end{bmatrix}\begin{bmatrix} 1 & \delta_2 \\ \delta_1/f & f \end{bmatrix} \tag{3}$$

Using matrix $[Y]$:

$$\begin{bmatrix} Y_{HH} & Y_{HV} \\ Y_{VH} & Y_{VV} \end{bmatrix} = Ae^{j\theta}\begin{bmatrix} S_{HH} & fS_{HV} \\ fS_{VH} & f^2S_{VV} \end{bmatrix} \tag{4}$$

$$\begin{bmatrix} M_{HH} & M_{HV} \\ M_{VH} & M_{VV} \end{bmatrix} = \begin{bmatrix} 1 & \delta_1/f \\ \delta_2 & 1 \end{bmatrix}\begin{bmatrix} Y_{HH} & Y_{HV} \\ Y_{VH} & Y_{VV} \end{bmatrix}\begin{bmatrix} 1 & \delta_2 \\ \delta_1/f & f \end{bmatrix} \tag{5}$$

Considering the reflection symmetry theory, the relationship between scattering measurement matrix $[M]$ and matrix $[Y]$ can be shown as:

$$\langle M_{HH}M_{HH}^*\rangle \approx \langle Y_{HH}Y_{HH}^*\rangle, \langle M_{VV}M_{VV}^*\rangle \approx \langle Y_{VV}Y_{VV}^*\rangle$$

$$\langle M_{HV}M_{HH}^*\rangle \approx \langle Y_{HV}Y_{HH}^*\rangle + \delta_2\langle Y_{HV}Y_{HH}^*\rangle + \frac{\delta_1}{f}\langle Y_{VV}Y_{HH}^*\rangle + 2\left(\frac{\delta_1}{f}\right)^*\langle Y_{HV}Y_{HV}^*\rangle \tag{6}$$

$$\langle M_{HV}M_{VV}^*\rangle \approx \langle Y_{HV}Y_{VV}^*\rangle + \delta_2\langle Y_{HH}Y_{VV}^*\rangle + \frac{\delta_1}{f}\langle Y_{VV}Y_{VV}^*\rangle + 2\delta_2^*\langle Y_{HV}Y_{HV}^*\rangle$$

The Amazon rainforest is used to observe the variation of backscattering during the mission life. For the C-band radar, this target could be considered as a stable rough surface, which equally scatters the incident radar electromagnetic waves in all directions. With use of quad-polarization SAR imagery of rainforest, the polarization distortion matrix can

be acquired and the crosstalk and amplitude-phase imbalance can be removed [23–25]. Although the natural distributed ground targets of Amazon rainforest can be well applied for removal of crosstalk and amplitude-phase imbalance, it is significant to assess the residual amplitude and phase error. When only amplitude imbalance is considered, the Equation (1) can be simplified as:

$$
\begin{bmatrix} M_{HH} & M_{HV} \\ M_{VH} & M_{VV} \end{bmatrix} = Ae^{j\theta} \begin{bmatrix} 1 & 0 \\ 0 & f_r \end{bmatrix} \begin{bmatrix} S_{HH} & S_{HV} \\ S_{VH} & S_{VV} \end{bmatrix} \begin{bmatrix} 1 & 0 \\ 0 & f_t \end{bmatrix} \tag{7}
$$

and by average:

$$
\begin{aligned}
\langle |M_{HH}|^2 \rangle &= A^2 \langle |S_{HH}|^2 \rangle \\
\langle |M_{HV}|^2 \rangle &= A^2 \langle |S_{HV}|^2 \rangle \\
\langle |M_{VH}|^2 \rangle &= A^2 \langle |S_{VH}|^2 \rangle \\
\langle |M_{VV}|^2 \rangle &= A^2 \langle |S_{VV}|^2 \rangle
\end{aligned} \tag{8}
$$

Taking the log of both sides of Equation (8), expression can be transformed to:

$$
\begin{aligned}
|M_{HH}|_L &= |A|_L + |S_{HH}|_L \\
|M_{HV}|_L &= |A|_L + |f_r|_L + |S_{HV}|_L \\
|M_{VH}|_L &= |A|_L + |f_t|_L + |S_{VH}|_L \\
|M_{VV}|_L &= |A|_L + +|f_r|_L + |f_t|_L |S_{VV}|_L
\end{aligned} \tag{9}
$$

Then the amplitude imbalance can be expressed as:

$$
\begin{aligned}
|f_r|_L &= \tfrac{1}{2} (\Delta f_\alpha - \Delta f_\beta) + \tfrac{1}{2} (|M_{VV}|_L - |M_{HH}|_L + |M_{HV}|_L - |M_{VH}|_L) \\
|f_t|_L &= \tfrac{1}{2} (\Delta f_\alpha + \Delta f_\beta) + \tfrac{1}{2} (|M_{VV}|_L - |M_{HH}|_L + |M_{HV}|_L - |M_{VH}|_L)
\end{aligned} \tag{10}
$$

where:

$$
\Delta f_\alpha = |S_{HH}|_L - |S_{VV}|_L \quad \Delta f_\beta = |S_{HV}|_L - |S_{VH}|_L \tag{11}
$$

Δf_α and Δf_β were related with the scattering amplitude characteristics of ground targets.

Similarly, by solving the cross-polarization and co-polarization of the measurement matrix, the phase imbalance can be expressed as:

$$
\begin{aligned}
\theta_r &= \tfrac{1}{2} (\Delta\theta_\alpha - \Delta\theta_\beta) + \tfrac{1}{2} \left(Phase(\langle M_{HV} M_{VH}^* \rangle) - Phase(\langle M_{HH} M_{VV}^* \rangle) \right) \\
\theta_t &= \tfrac{1}{2} (\Delta\theta_\alpha + \Delta\theta_\beta) - \tfrac{1}{2} \left(Phase(\langle M_{HV} M_{VH}^* \rangle) + Phase(\langle M_{HH} M_{VV}^* \rangle) \right)
\end{aligned} \tag{12}
$$

where:

$$
\begin{aligned}
\Delta\theta_\alpha &= Phase(\langle S_{HH} S_{VV}^* \rangle) \\
\Delta\theta_\beta &= Phase(\langle S_{HV} S_{VH}^* \rangle)
\end{aligned} \tag{13}
$$

$\Delta\theta_\alpha$ and $\Delta\theta_\beta$ were related with the scattering phase characteristics of ground targets.

Theoretically, the amplitude and phase imbalance can be well removed. Due to the system measurement errors, some residual amplitude and phase error still affects the imagery quality. It is also very important to assess the influence of residual amplitude and phase error for GF-3 quad-polarization SAR. Series of quad-polarization SAR imagery of rainforest were performed to amplitude and phase imbalance removal. Quad-polarization SAR sub-imagery of Amazon rainforest were shown in Figure 2. The details of used Amazon rainforest of GF-3 SAR imagery was listed in Table 2. For the C-band radar, Amazon rainforest could be considered as a rough surface, which equally scatters the incident radar electromagnetic waves in all directions.
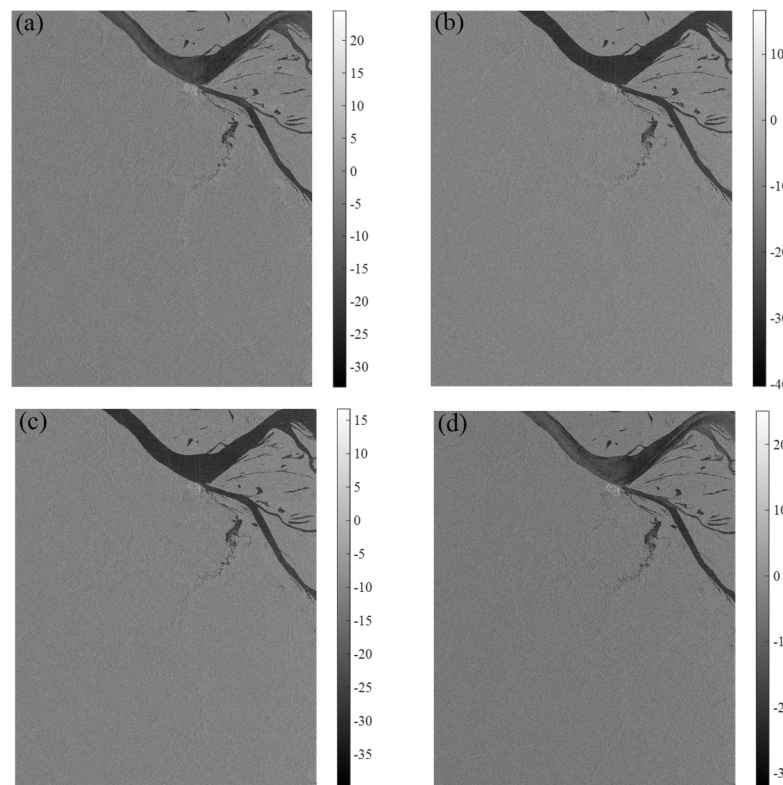
Figure 2. Quad-polarization SAR sub-imagery of rainforest used in this study: (**a**–**d**) Represents the HH, HV, VH, VV polarization, respectively.

Table 2. Parameters of used datasets in this study.

| Sensor	Wave Code	Incident Angle	Latitude	Longitude	Acquisition Time
GF-3 SAR	191	23.81–26.48°	−2.86°	−66.75°	7 December 2019, 10:17:18
GF-3 SAR	189	19.95–22.75°	0.71°	−67.56°	21 October 2021, 22:43:35
GF-3 SAR	203	39.51–40.76°	0.77°	−68.22°	2 November 2021, 10:17:41

(2)   Ocean

Ocean surface is a perfect naturally homogeneous scene for SAR calibration. The scattering characteristics of ocean surface in SAR imagery totally attributes to surface scattering. It is different from rainforest, where there is sum of surface scattering, secondary scattering and volume scattering. The scattering mechanism difference also affects the performance of SAR imagery calibration for different measurement scenes. Moreover, numerous acquisitions over open ocean are therefore advantageous for operational application. For retrieval of wind and waves, it is revealed that the performance of ocean surface calibration method was more effective than other methods [26]. Bragg scattering model, two scale model (TSM), three scale model (MSM), small slope approximation (SSA) and integral expansion method (IEM), etc., are proposed to analyze the scattering characteristic for difference radar incidence angle and sea state. For now, ocean surface calibration method was focused, and relevant study shows the feasibility and capability of ocean surface calibration method for SAR imagery [27–29].

3. Results

3.1. Assessment of Amplitude and Phase Imbalance

It should be noted that the amplitude and phase imbalance can be well removed using GF-3 SAR imagery of rainforest for validation. For wind speed retrieval, the response of amplitude and phase imbalance to sea state and radar parameters is still in doubt. By collocating with ECMWF wind vector, scenes of GF-3 SAR wave mode imagery were collected among the amplitude and phase imbalance of the whole channel representing the amplitude and phase error of VV channel relative to HH channel, which are shown in Figure 3. For GF-3 SAR wave mode imagery, the amplitude imbalance variation of receive channel was basically consistent with corresponding transmit channel in Figure 3. Additionally, the phase imbalance variation of receive channel causes much deviation between receive and transmit channel in Figure 3. Moreover, the phase imbalance of receive channel can reach 20°, instead, the phase imbalance of transmit channel settles in 0°.


(**a**)

(**b**)
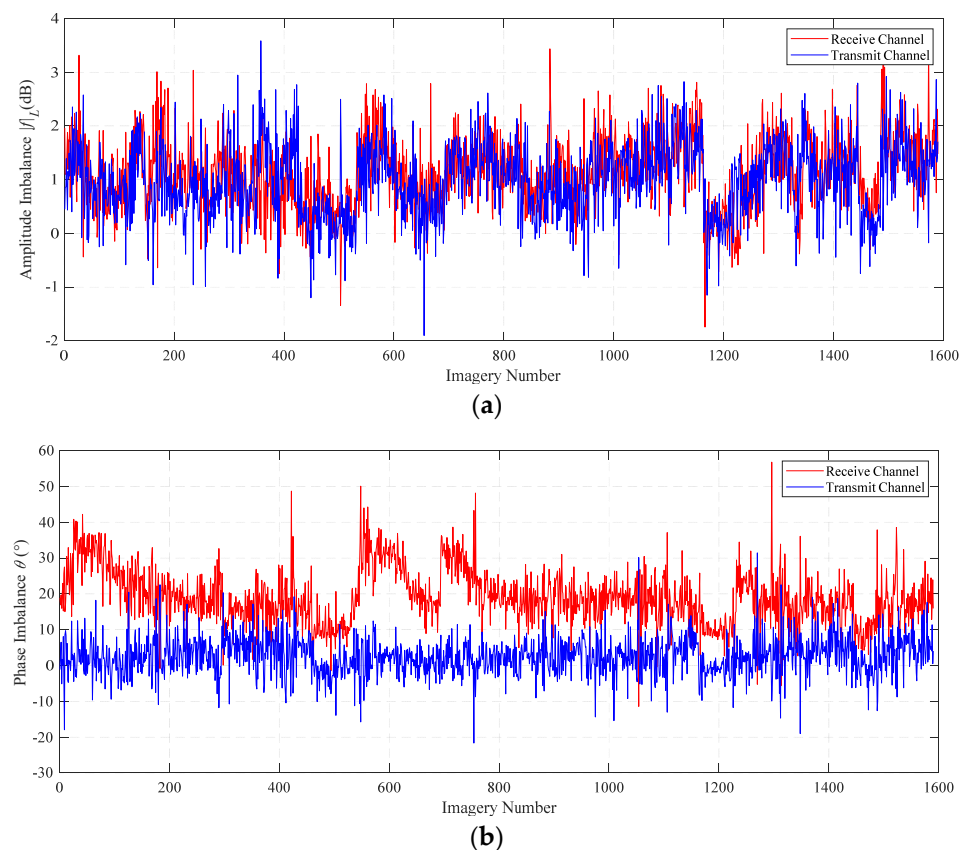
Figure 3. Series of amplitude imbalance (**a**) and phase imbalance (**b**) for receive and transmit channel from GF-3 SAR imagery of sea surface observation.

Figure 4a,b represent the amplitude and phase imbalance relative to wind speed for both transmit and receive channel, respectively. It can be found that the amplitude imbalance is negatively proportional to wind speed for both transmit and receive channel. Obviously, the amplitude imbalance can reach to (1.2 ± 0.7) dB in low wind speed zone, and decreased to (0.6 ± 0.4) dB in medium-high wind speed zone. Moreover, the phase imbalance of receive channel settled in $(19.7 \pm 9.7)°$ in low-medium wind speed zone and decreased to $(11.7 \pm 7.7)°$ in high wind speed zone. Unlike receive channel, the phase imbalance of transmit channel settled in $(1.9 \pm 5.6)°$ in low-medium wind speed zone and deteriorated to $(-2.6 \pm 2.8)°$ in high wind speed zone.
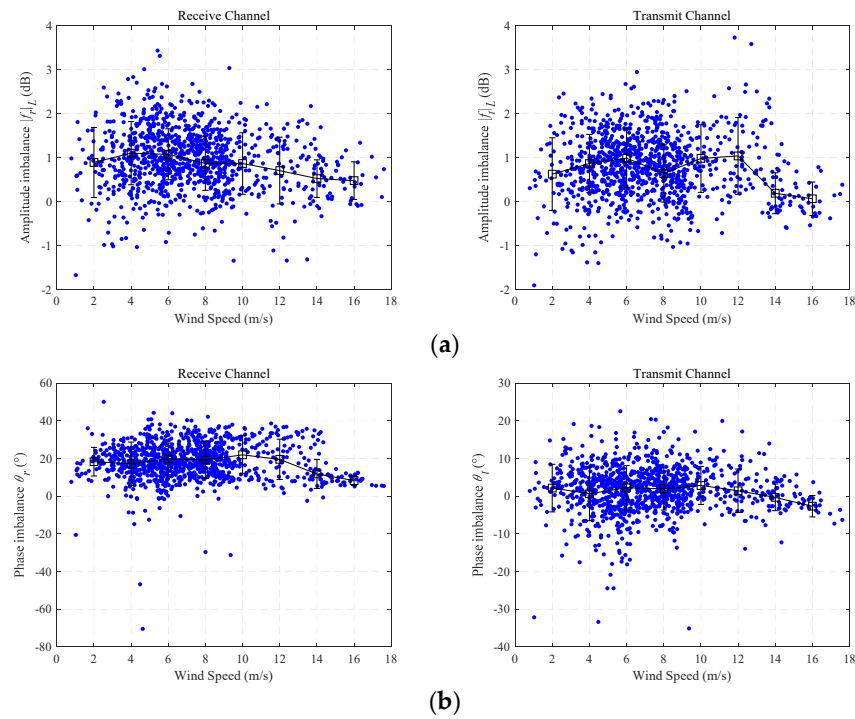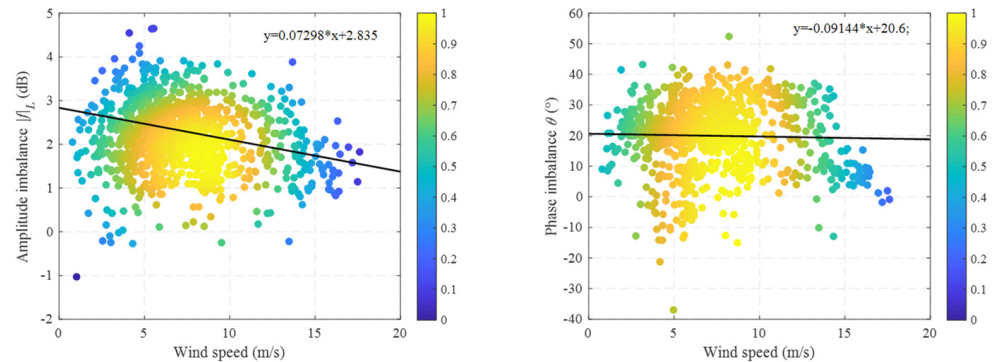
Figure 4. (**a**,**b**) The amplitude and phase imbalance of GF-3 SAR imagery of sea surface observation for receive and transmit channel. Upper row represents the amplitude imbalance variation relative to wind speed, and down row represents the phase imbalance variation relative to wind speed.

Besides wind speed, the radar parameter of incidence angle was also worthwhile to investigate. Figure 5 presents the amplitude and phase imbalance relative incidence angle for both transmit and receive channel, respectively. It can be seen that the amplitude of transmitting channel is slightly larger than that of receiving channel. Moreover, the phase deviation of the transmitting channel is smaller than that of the receiving channel.
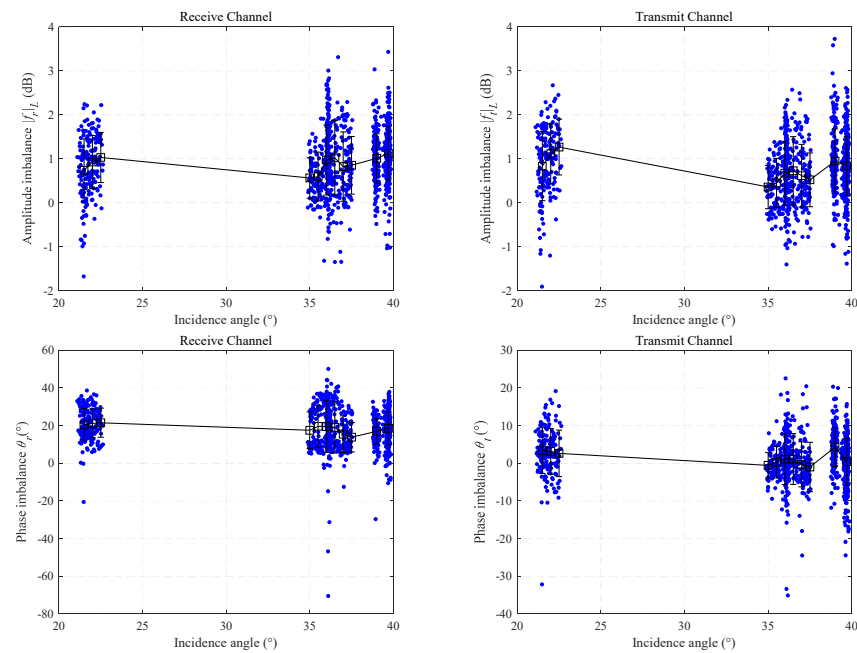
Figure 5. The amplitude and phase imbalance variation relative to incidence angle. Same with Figure 4.

Actually, the total amplitude and phase imbalance can be attributed to the sum of transmit and receive channel. With combination of transmit and receive channel, the amplitude and phase imbalance relative to wind speed were shown in Figure 6. Slopes of linear regression are 0.07298 for amplitude imbalance and –0.09144 for phase imbalance, respectively. Since wind speed increases, the amplitude imbalance decreases proportionally, and the minimum value was still greater than 1 dB and phase imbalance was constant as $20°$.


Figure 6. The empirical fitting result of amplitude and phase imbalance relative to wind speed.

In SAR observation of sea surface, the phase distribution of sea surface waves was regarded as random. It should be noted that the imagery amplitude of sea surface was highly related with wind speed using CMOD model. So the influence of amplitude imbalance on wind speed retrieval was aimed to assess in this paper. The use of phase imbalance was also revealed to acquire sea surface current for GF-3 multi-channel SAR measurement, which is quietly different with quad-polarization SAR [30]. For wind field inversion, it is interesting to assess influence of amplitude and phase imbalance on wind direction retrieval.
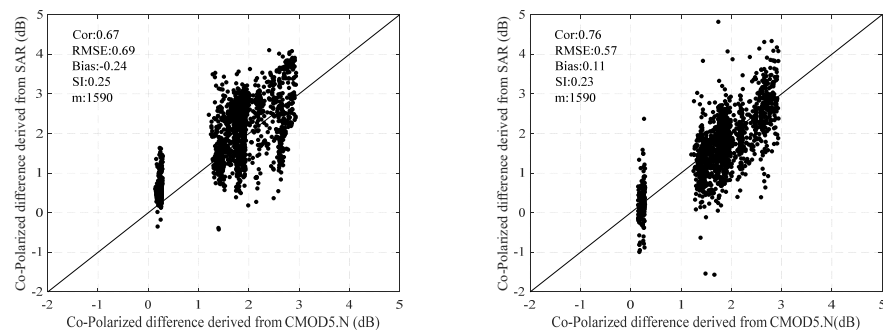
3.2. Influence of Residual Amplitude Error on Wind Speed Retrieval

In fact, the polarization difference of sea surface scattering was confused in the total amplitude and phase imbalance. In order to explore the residual amplitude and phase error from channel imbalance, the theory bias caused by co-polarization difference of sea surface scattering deserve to be removed. To assess the influence of residual amplitude error on wind speed retrieval, the scattering characteristics of sea surface for HH and VV polarization need to be removed firstly. Using CMOD5.N model, the response of polarization NRCS relative to incidence angle and wind speed was present. It is noted that the polarization ratio was re-fitted using GF-3 SAR wave mode imagery. Figure 7a shows the NRCS of HH and VV polarization increased with increase of wind speed at incidence angles of $30°$, $40°$, $50°$, respectively. In addition, the NRCS of HH and VV polarization varied with increase of relative wind direction at wind speed 5 m/s, 10 m/s, 15 m/s in Figure 7b, respectively.

Taking sea surface scattering characteristics of CMOD5.N as theoretical value, the influence of polarization difference was removed from total amplitude and phase error for both transmit and receive channel. For wind speed, the NRCS was mainly input in retrieval model once incidence angle and wind direction were confirmed. So the residual amplitude error was mainly focused in this section. After the co-polarization response difference removal, the residual amplitude was proposed. The co-polarization difference from SAR was compared with CMOD5.N in Figure 8. For VV polarization, the correlation between co-polarization difference from GF-3 SAR and CMOD5.N increased from 0.67 to 0.76, with use of residual amplitude correction.
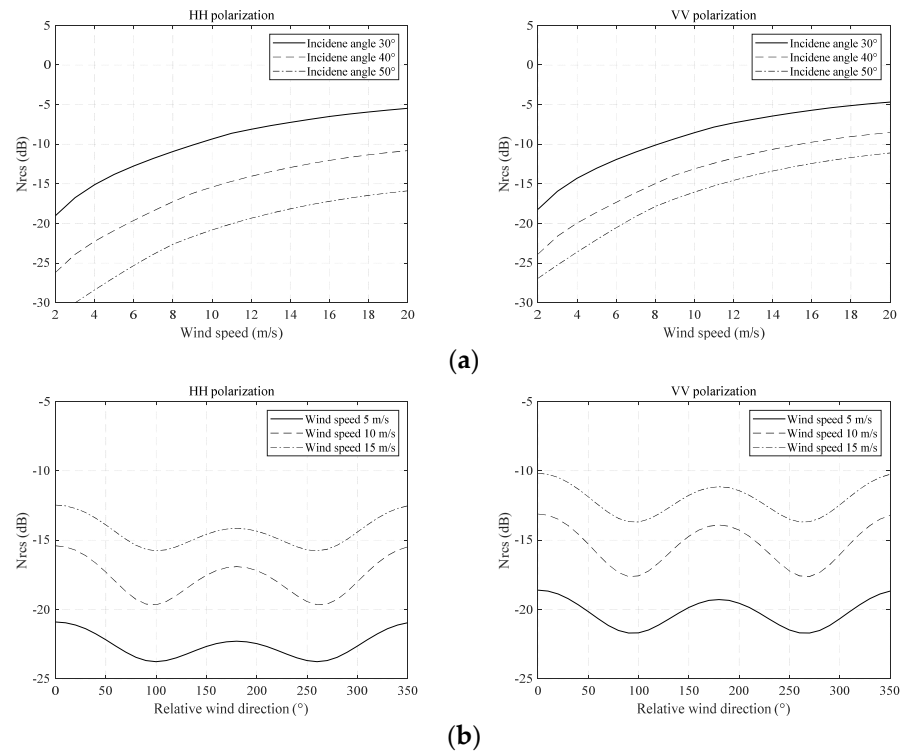
Figure 7. (**a**,**b**) The NRCS of sea surface variation relative to wind speed and relative wind direction. Wind speed ranges from 2 m/s to 20 m/s and relative wind direction ranges from 0° to 350°. Upper row presents NRCS variation at relative wind direction 0°, lower row presents NRCS variation at incidence 40°.

Figure 8. The comparison between co-polarization difference from CMOD5.N and GF-3 SAR. Left column presents the original SAR measurement; right column presents the compensated SAR measurement with removal of residual amplitude error.

As known, the wind speed was highly related with sea surface microwave scattering caused by wind-driven sea surface roughness. The backscatter amplitude presents the sea surface NRCS, which affects the wind speed retrieval. Moreover, the phase was not directly applied to wind speed retrieval and usually neglected in ocean SAR application. To explore the influence of residual amplitude and phase error on wind speed retrieval, CMOD5.N model was proposed to derive wind speed firstly. It is noted that CMOD5.N was well applied for VV polarization SAR imagery. To acquire the wind speed using HH polarization, the Polarization Ratio (*PR*) model was combined with CMOD5.N model.

$$PR = \frac{\sigma_0^{VV}}{\sigma_0^{HH}} \qquad (14)$$

It is noted that the σ_0^{VV} represents the NRCS of sea surface in VV polarization; σ_0^{HH} represents the NRCS of sea surface in HH polarization. Several PR models were proposed in recent studies [31,32]. The *PR* model can be acquired with the following:
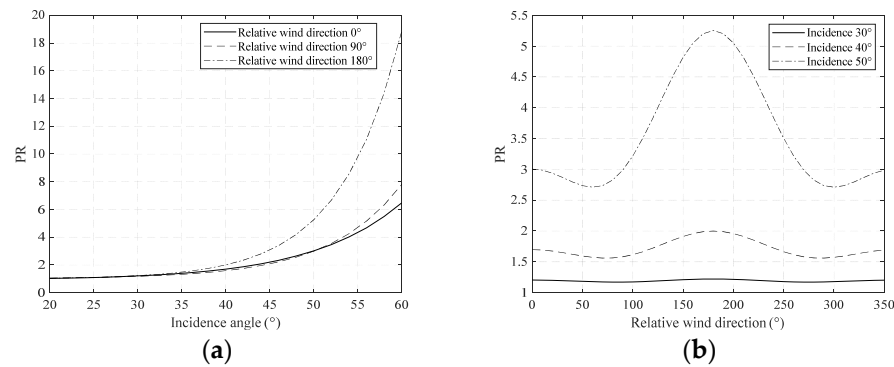
$$PR(\theta, \phi) = C_0(\theta) + C_1(\theta)\cos\phi + C_2(\theta)\cos 2\phi \tag{15}$$

$$C_0(\theta) = \frac{PR(\theta, 0) + PR(\theta, \pi) + 2PR(\theta, \pi/2)}{4} \tag{16}$$

$$C_1(\theta) = \frac{PR(\theta, 0) - PR(\theta, \pi)}{2} \tag{17}$$

$$C_2(\theta) = \frac{PR(\theta, 0) + PR(\theta, \pi) - 2PR(\theta, \pi/2)}{4} \tag{18}$$

Zhang [32] proposed a novel PR model with RADATSAT-2 quad-polarization data. It is also proven that the model was validated for wind speed from HH polarization SAR imagery. In this study, we take Zhang's PR model as reference for wind speed retrieval of GF-3 HH polarization SAR, which is shown in Figure 9.


Figure 9. The PR model refitted from GF-3 SAR imagery: (**a**) Represents the PR variation relative to incidence angle; (**b**) Represents the PR variation relative to relative wind direction.

As shown in Figure 10, the SAR-derived wind speed retrieval precision was compared with on-site wind speed provided by ECMWF. To assess the fitting performance, the correlation coefficient (Cor), root mean square error (RMSE), Bias, and Scattering index (SI) were selected as features. The performance of SAR wind speed retrieval was fitted with a Cor of 0.82, RMSE of 1.86 and a Cor of 0.86; RMSE of 1.71 for both of VV and HH polarization, respectively.
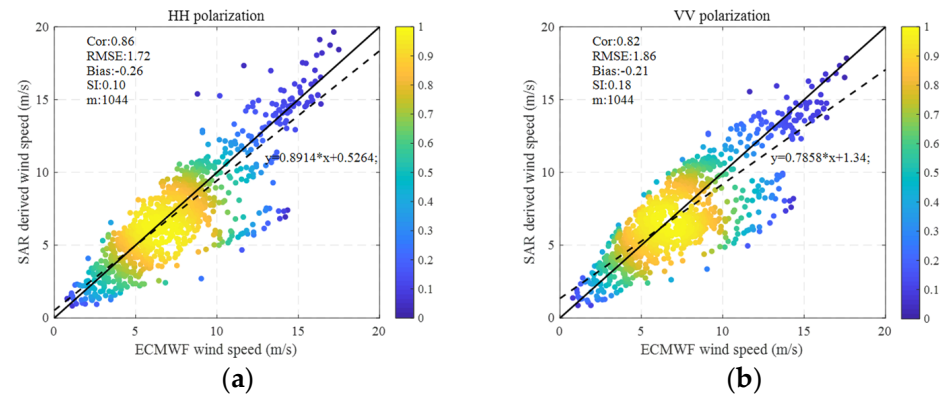

Figure 10. Wind speed retrieval precision for GF-3 SAR HH and VV polarization. The SAR-derived wind speed was compared with on-site wind speed provided by ECMWF: (**a**) CMOD5.N+PR; (**b**) CMOD5.N. The color represents the density of scatter points.

To assess the influence of residual amplitude error on wind speed retrieval, it is important to quantify the residual amplitude error as variables of wind speed. Figure 11 established the empirical fitting results between residual amplitude error and wind speed. It can be seen that the residual amplitude error represents weakly correlation relative to wind speed. The residual amplitude error performed as random. However, it cannot be neglected for the purpose to develop the retrieval precision of wind speed. Moreover, the relationship between polarization isolation and residual amplitude error was also explored. It is founded that the slopes of linear regression was −0.113. The polarization isolation of GF-3 SAR was designed as −35 dB.
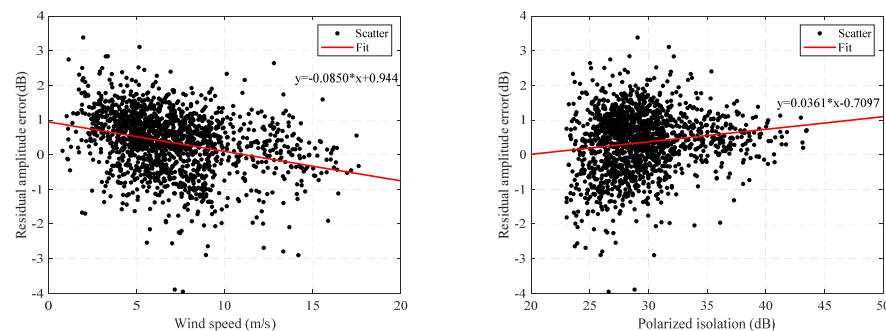
Figure 11. The residual amplitude error variation relative to wind speed and polarization isolation.

According to the empirical relationship from Figure 11, the NRCS derived from SAR was compared with CMOD5.N model with correction of residual amplitude error as shown in Figure 12. It can be seen that the corrected NRCS was highly related with CMOD5.N. To further explore the influence of residual amplitude error, the wind speed was retrieved from corrected NRCS, with Cor of 0.86, RMSE of 1.64. Comparing with original retrieval results of Figure 10b, the correction of residual amplitude error will improve the retrieval precision of VV polarization GF-3 SAR.
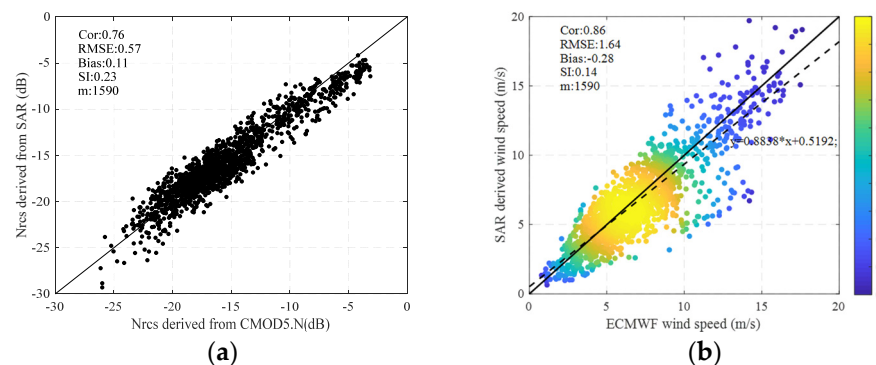
Figure 12. Performance of corrected NRCS on wind speed retrieval: (**a**) NRCS derived from SAR variation relative to CMOD5.N model; (**b**) The SAR-derived wind speed variation relative to ECMWF wind speed.

The performance of residual amplitude error correction on wind speed retrieval is listed in Table 3. Using correction of residual amplitude error of GF-3 SAR imagery for sea surface, the retrieval precision of wind speed improved, with an increase of Cor from 0.82 to 0.86. Moreover, the RMSE, Bias, and SI decreased from 0.86 to 1.64, from −0.21 to −0.28 and from 0.18 to 0.14, respectively. Various indicators of assessment result precision shows remarkable improvement.

Table 3. Performance of residual amplitude error correction on wind speed retrieval.

	Cor	RMSE	Bias	SI
No correction	0.82	1.86	−0.21	0.18
Correction	0.86	1.64	−0.28	0.14

3.3. Influence of Residual Amplitude and Phase Error on Wind Direction Retrieval

Few studies focused on the wind direction retrieval directly from quad-polarization SAR instead of external on-site wind direction. A method was proposed to inverse wind direction from Radasat-2 quad-polarization SAR by establishing the discriminant rule from polarization correlation coefficient to wind direction [8]. As shown in Figure 13, the performance of polarization correlation coefficient ρ was presented as a Sine curve. The correlation coefficient ρ_{HHHV} and ρ_{VVHV} were denoted as:

$$\rho_{PPHV} = \frac{\langle S_{PP} \Delta S_{HV}^* \rangle}{\sqrt{\langle |S_{PP}|^2 \rangle \langle |S_{HV}|^2 \rangle}} \tag{19}$$
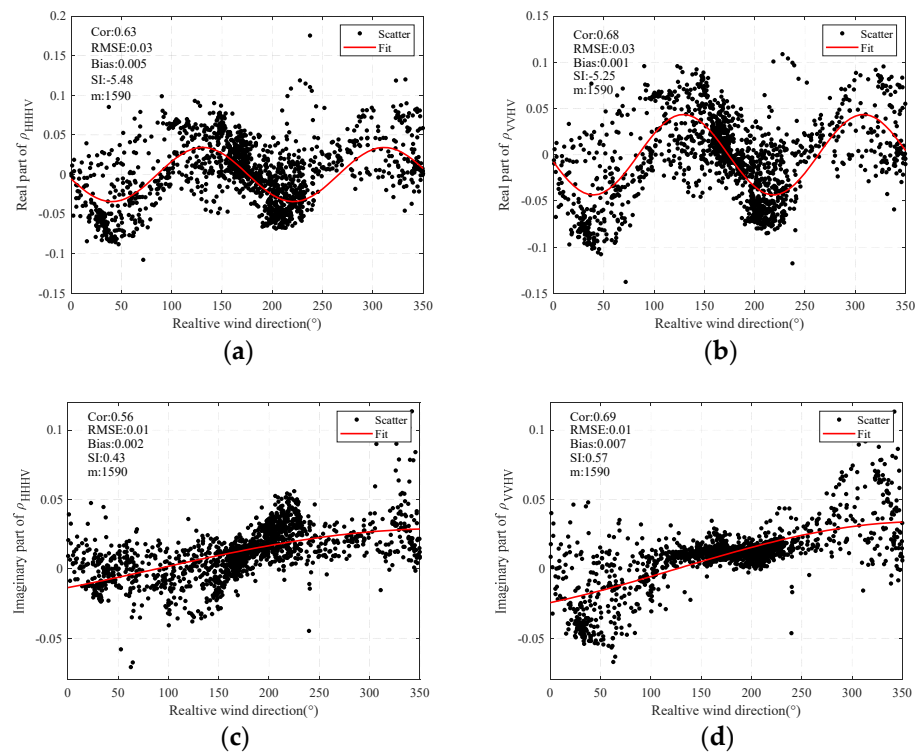
Figure 13. Performance of polarization correlation coefficient ρ variation relative to relative wind direction: (**a**) Real part of ρ_{HHHV}; (**b**) Real part of ρ_{VVHV}; (**c**) Imaginary part of ρ_{HHHV}; (**d**) Imaginary part of ρ_{VVHV}.

The S present the polarization scattering matrix, the pp represent the polarization channel; HH and VV polarization were selected in this paper, the < > present the average operation. Comparing the fitting performance of ρ_{HHHV} and ρ_{VVHV}, it is revealed that the ρ_{VVHV} was prior to facilitate the selection of the relative wind direction.

In study [8], the odd symmetry characteristic of polarization correlation coefficient ρ was applied to acquire the selection of the relative wind direction among the four relative wind direction solutions. The criteria are as follows:

From Table 4, it is concluded that the wind direction was not directly derived from SAR imagery, but confirmed the selection range of wind direction from CMOD5.N model. Although the ρ error was attributed to residual amplitude and phase error can be assessed, the influence of residual amplitude and phase error on selection of wind direction from

Table 4 can be neglected. It is noted that the wind speed is highly related with NRCS, which can be attributed to the imagery amplitude. Moreover, the imagery phase of sea surface is regarded as random from –pi to pi. This is why few studies focused on the application of imagery phase. This can also explain why rainforest can be used for sea surface imagery calibration in this study. It is because wind speed mainly depended on the imagery intensity, not imagery phase. However, for wind direction retrieval, the applicability of rainforest needs to be discussed, because the reflection symmetry theory was not satisfied for the sea surface. As survey and statistics show, few studies try to propose the wind direction retrieval algorithm using imagery phase, and the retrieval precision was not satisfying at all. It can be explained that the scattering of rainforest follows the reciprocity and reflection symmetry theory; the phase error between different polarization channels and crosstalk were calibrated using four polarization SAR imagery of rainforest. However, reflection symmetry theory was not satisfied for the sea surface, which caused a large bias in wind direction retrieval.

Table 4. Discriminant rule from polarization correlation coefficient to wind direction.

Real Part of ρ	Imagery Part of ρ	Relative Wind Direction
<0	>0	$-180° < \Phi < -90°$
>0	>0	$-90° < \Phi < 0°$
<0	<0	$0° < \Phi < 90°$
>0	<0	$90° < \Phi < 180°$

4. Discussion

For now, the calibration of GF-3 SAR imagery for sea surface observation has been focused. Several studies aimed to recalibrate the NRCS using rainforest or sea surface. However, the error source of NRCS was neglected. The usability of these methods was also not discussed yet. In this paper, we aimed to analyze the residual amplitude and phase error for sea surface when using rainforest as calibration target. Moreover, the influence of residual amplitude and phase error on NRCS was quantitatively assessed. It is verified that with correction of residual amplitude and phase error, the retrieval precision of wind speed using GF-3 SAR imagery was improved remarkably. For wind speed retrieval, the CMOD model was widely used:

$$U_{10} = CMOD(Nrcs, inc, phi) \tag{20}$$

It is noted that the *Nrcs* represents the observed value from SAR imagery, *inc* represents the radar incidence angle, and the *phi* represents the relative wind direction relative to antenna look angle. Obviously, the NRCS bias caused by residual amplitude and phase error has not been taken into consideration yet. It is suggested to take it as one of the key parameters in CMOD for future study.

5. Conclusions

GF-3 quad-polarization SAR was widely used for wind speed retrieval. This requires a precise NRCS from SAR imagery. SAR backscattering variation is subject to various radar loading state, atmospheric phenomena, and sea surface dynamics characteristics. To acquire the precise NRCS from SAR imagery, the active calibrator was usually used for calibration. However, it is questionable that this calibration method was well applied for high Signal Noise Ratio (SNR) condition. To develop the calibration precision of SAR, the rainforest was almost used for NRCS calibration instead of active calibrator or corner reflector. However, the applicability of rainforest calibration was not widely assessed, especially for ocean quantitative remote sensing application.

In this paper, the amplitude and phase imbalance were selected to characterize the calibration error of GF-3 quad-polarization SAR. Variation of amplitude and phase imbalance for transmit and receive channel were assessed against collocated wind speed and

incidence angle. Considering the polarization difference of VV channel relative to HH channel, the residual amplitude and phase error was found to be closely related to wind speed and polarization isolation. Correction of residual amplitude and phase error were employed to improve the retrieval precision of wind vector. It is revealed that the wind speed retrieval precision of VV polarization improved with correction of residual amplitude error. In addition, the influence of residual amplitude and phase error on wind direction retrieval can be neglected. Thus, it is concluded that correction of amplitude and phase error has the potential to improve wind vector retrievals from quad-polarization SAR.

Author Contributions: Conceptualization, X.W. and B.H.; methodology, Y.H.; data curation, X.Y.; writing—review and editing, J.Y. and J.D. All authors have read and agreed to the published version of the manuscript.

Institutional Review Board Statement: Not applicable.

Informed Consent Statement: Informed consent was obtained from all subjects involved in the study.

Conflicts of Interest: The authors declare no conflict of interest.

References

1. Hasselmann, K.; Hasselmann, S. On the nonlinear mapping of an ocean wave spectrum into a synthetic aperture radar image spectrum and its inversion. *J. Geophys. Res. Earth Surf.* **1991**, *96*, 10713–10729. [CrossRef]
2. Chapron, B.; Johnsen, H.; Garello, R. Wave and wind retrieval from sar images of the ocean. *Ann. Telecommun.* **2001**, *56*, 682–699. [CrossRef]
3. Li, X.-M.; Lehner, S.; Bruns, T. Ocean Wave Integral Parameter Measurements Using Envisat ASAR Wave Mode Data. *IEEE Trans. Geosci. Remote Sens.* **2010**, *49*, 155–174. [CrossRef]
4. Vachon, P.W.; Dobson, F.W. Validation of wind vector retrieval from ERS-1 SAR images over the ocean. *Glob. Atmos. Ocean. Syst.* **1996**, *5*, 177–187.
5. Shao, W.; Sheng, Y.; Sun, J. Preliminary Assessment of Wind and Wave Retrieval from Chinese Gaofen-3 SAR Imagery. *Sensors* **2017**, *17*, 1705. [CrossRef] [PubMed]
6. Wan, Y.; Shi, X.; Dai, Y.; Li, L.; Qu, X.; Zhang, X. Research on Wind Speed Inversion Method for X-Band Networked SAR Satellite. *J. Mar. Sci. Eng.* **2020**, *8*, 626. [CrossRef]
7. Shao, W.; Li, X.; Hwang, P.; Zhang, B.; Yang, X. Bridging the gap between cyclone wind and wave by C -band SAR measurements. *J. Geophys. Res. Oceans* **2017**, *122*, 6714–6724. [CrossRef]
8. Zhang, B.; Perrie, W.; Vachon, P.W.; Li, X.; Pichel, W.G.; Guo, J.; He, Y. Ocean Vector Winds Retrieval From C-Band Fully Polarimetric SAR Measurements. *IEEE Trans. Geosci. Remote Sens.* **2012**, *50*, 4252–4261. [CrossRef]
9. Zhang, R.W.; Yan, W.; Ai, W.-H.; Shuo, M.A. A Method of Ocean Surface Wind Direction Retrievals for Airborne SAR Images Based on Gabor Wavelet Transform. *J. Microw.* **2011**, *27*, 79–83.
10. Ai, W.-H.; Yi, K.; Xian-Bin, Z. Ocean surface wind direction retrieval from multi-polarization airborne SAR based on wavelet. *Acta Phys. Sin.* **2012**, *61*, 148403. [CrossRef]
11. Fan, K.; Huang, W.; He, M.; Fu, B. Wind direction analysis over the ocean using SAR imagery. *J. Inf. Comp.* **2008**, *5*, 223–231.
12. Wang, L.; Han, B.; Yuan, X.; Lei, B.; Ding, C.; Yao, Y.; Chen, Q. A Preliminary Analysis of Wind Retrieval, Based on GF-3 Wave Mode Data. *Sensors* **2018**, *18*, 1604. [CrossRef] [PubMed]
13. Wang, H.; Li, H.; Lin, M.; Zhu, J.; Wang, J.; Li, W.; Cui, L. Calibration of the Copolarized Backscattering Measurements from Gaofen-3 Synthetic Aperture Radar Wave Mode Imagery. *IEEE J. Sel. Top. Appl. Earth Obs. Remote Sens.* **2019**, *12*, 1748–1762. [CrossRef]
14. Zhu, S.; Shao, W.; Marino, A.; Sun, J.; Yuan, X. Semi-empirical algorithm for wind speed retrieval from Gaofen-3 quad-polarization strip mode SAR data. *J. Ocean. Univ. China* **2020**, *19*, 23–35. [CrossRef]
15. Jiang, S.; Qiu, X.; Han, B.; Hu, W. A Quality Assessment Method Based on Common Distributed Targets for GF-3 Polarimetric SAR Data. *Sensors* **2018**, *18*, 807. [CrossRef]
16. Shangguan, S.; Qiu, X.; Fu, K.; Lei, B.; Hong, W. GF-3 Polarimetric Data Quality Assessment Based on Automatic Extraction of Distributed Targets. *IEEE J. Sel. Top. Appl. Earth Obs. Remote Sens.* **2020**, *13*, 4282–4294. [CrossRef]
17. Xu, L.; Li, W.; Cui, L.; Tong, Q.; Chen, J. Study on the impact of Polarimetric calibration errors on terrain classification with PolInSAR. In Proceedings of the Geoscience and Remote Sensing Symposium, Beijing, China, 10–15 July 2016; pp. 4722–4725.
18. Correia, A.H.; da Costa Freitas, C.; Mura, J.C. Evaluation of the influence of the polarimetric calibration process on the H/A/alpha decomposition. In Proceedings of the 2010 IEEE International Geoscience and Remote Sensing Symposium, Honolulu, HI, USA, 25–30 July 2010; pp. 2039–2042.

19. Hu, D.; Qiu, X.; Lei, B.; Xu, F. Analysis of crosstalk impact on the Cloude-decomposition-based scattering characteristic. *J. Radars* **2017**, *6*, 221–228.

20. Freeman, A.; Shen, Y.; Werner, C. Polarimetric SAR calibration experiment using active radar calibrators. *IEEE Trans. Geosci. Remote Sens.* **1990**, *28*, 224–240. [CrossRef]

21. Li, H.; Mouche, A.; Stopa, J.E.; Chapron, B. Calibration of the normalized radar cross section for sentinel-1 wave mode. *IEEE Trans. Geosci. Remote Sens.* **2018**, *57*, 1514–1522. [CrossRef]

22. Van Zyl, J. Calibration of polarimetric radar images using only image parameters and trihedral corner reflector responses. *IEEE Trans. Geosci. Remote Sens.* **1990**, *28*, 337–348. [CrossRef]

23. Barnes, R.M. Polarimetric Calibration Using Distributed Clutter. In Proceedings of the SPIE—The International Society for Optical Engineering, Orlando, FL, USA, 14 August 1989; Volume 1101, pp. 53–59.

24. Freeman, A.; Werner, C.; Shen, Y. Calibration of multipolarisation imaging radar. *Remote Sens.* **1988**, *1*, 335–339.

25. Whitt, M.W.; Ulaby, F.T. *A General Polarimetric Calibration Technique*; University of Michigan, Radiation Laboratory: Ann Arbor, MI, USA, 1989.

26. Verspeek, J.; Portabella, M.; Stoffelen, A.; Verhoef, A.; Calibration and Validation of ASCAT Winds. The EUMETSAT Network of Satellite Application Facilities, 11 July 2011. Available online: https://cdn.knmi.nl/system/data_center_publications/files/000/069/426/original/calibration_and_validation_of_ascat_winds_5_1.pdf?1495621762 (accessed on 30 May 2013).

27. Yan, Q.; Zhang, J.; Fan, C.; Wang, J.; Meng, J. Study of sea-surface slope distribution and its effect on radar backscatter based on Global Precipitation Measurement Ku-band precipitation radar measurements. *J. Appl. Remote Sens.* **2018**, *12*, 016006. [CrossRef]

28. Romeiser, R.; Alpers, W.; Wismann, V. An improved composite surface model for the radar backscattering cross section of the ocean surface: 1. Theory of the model and optimization/validation by scatterometer data. *J. Geophys. Res. Earth Surf.* **1997**, *102*, 25237–25250. [CrossRef]

29. Romeiser, R.; Alpers, W. An improved composite surface model for the radar backscattering cross section of the ocean surface: 2. Model response to surface roughness variations and the radar imaging of underwater bottom topography. *J. Geophys. Res. Earth Surf.* **1997**, *102*, 25251–25267. [CrossRef]

30. Shang, M.; Qiu, X.; Han, B.; Yang, J.; Zhong, L.; Ding, C.; Hu, Y. The space-time variation of phase imbalance for GF-3 azimuth multichannel mode. *IEEE J. Sel. Top. Appl. Earth Obs. Remote Sens.* **2020**, *13*, 4774–4788. [CrossRef]

31. Elfouhaily, T. Physical modeling of electromagnetic backscatter from the ocean surface. In *Application to Retrieval of Wind Fields and Wind Stress by Remote Sensing of the Marine Atmospheric Boundary Layer*; Dépt. d'Océanogr. Spatiale, l'Inst. Français Rec. l'Exploitation Mer (IFREMER): Plouzane, France, 1997.

32. Zhang, B.; Perrie, W.; He, Y. Wind speed retrieval from RADARSAT-2 quad-polarization images using a new polarization ratio model. *J. Geophys. Res. Ocean.* **2011**, *116*, C8. [CrossRef]